



ATLAS Note

ATLAS-CONF-2019-018

20th May 2019



Search for direct stau production in events with two hadronic tau leptons in $\sqrt{s} = 13$ TeV pp collisions with the ATLAS detector

The ATLAS Collaboration

A search for the direct production of the supersymmetric partners of tau leptons (staus) in final states with two hadronically decaying tau leptons is presented. The analysis uses a dataset of pp collisions corresponding to an integrated luminosity of 139 fb^{-1} , recorded with the ATLAS detector at the Large Hadron Collider at a centre-of-mass energy of 13 TeV. No significant deviation from the expected Standard Model background is observed. Limits are derived in scenarios of direct production of two mass-degenerate staus in simplified models with each stau decaying into the lightest neutralino and one tau lepton. Stau masses from 120 GeV to 390 GeV are excluded at 95% confidence level for a massless lightest neutralino.

1 Introduction

Supersymmetry (SUSY) [1–7] postulates the existence of superpartners, referred to as *sparticles*, whose spin differs by one half unit from each corresponding Standard Model (SM) particle. In models that conserve R -parity [8], sparticles are always produced in pairs, and the lightest supersymmetric particle (LSP) is stable and provides a dark-matter candidate [9, 10].

In SUSY models, the sector of sparticles with only electroweak interactions contains charginos ($\tilde{\chi}_i^\pm, i = 1, 2$ in order of increasing masses), neutralinos ($\tilde{\chi}_j^0, j = 1, 2, 3, 4$ in order of increasing masses), charged sleptons ($\tilde{\ell}$), and sneutrinos ($\tilde{\nu}$). Charginos and neutralinos are the mass eigenstates formed from the linear superpositions of the superpartners of the charged and neutral Higgs bosons and electroweak gauge bosons. The sleptons are the superpartners of the charged leptons and are referred to as left or right ($\tilde{\ell}_L$ or $\tilde{\ell}_R$) depending on the chirality of their SM partners. The slepton mass eigenstates are a mixture of $\tilde{\ell}_L$ and $\tilde{\ell}_R$, and are labelled as $\tilde{\ell}_1$ and $\tilde{\ell}_2$ (with $\tilde{\ell}_k, k = 1, 2$ in order of increasing masses). In this work, the scalar superpartner of the left-handed tau lepton (the stau-left) and right-handed tau lepton (stau-right) are considered to be mass degenerate.

Final states with tau leptons originating from stau decays are of particular interest for SUSY searches. Models with light staus can lead to a dark-matter relic density consistent with cosmological observations [11] and light sleptons in general could play a role in the co-annihilation of neutralinos [12, 13]. sleptons are expected to have masses of order 100 GeV in gauge-mediated [14–16] and anomaly-mediated [17, 18] SUSY breaking models.

In some scenarios the direct production of sleptons can dominate at the Large Hadron Collider (LHC) with respect to the production of squarks and gluinos. In the simplified models studied in this note, the lightest neutralino is the LSP and purely bino, and the two charged staus are assumed to be mass-degenerate. The left- and right-handed staus decay with a 100 % branching fraction to a bino-like neutralino ($\tilde{\tau}_{R,L}^\pm \tilde{\tau}_{R,L}^- \rightarrow \tilde{\chi}_1^0 \tau^\pm$). All sparticles other than those explicitly mentioned here are assumed to be inaccessible at the LHC energy. This note focuses on the direct production of a stau ($\tilde{\tau}$) pair, leading to the final state illustrated in Figure 1.

Signal events are characterised by the presence of exactly two tau leptons and large missing transverse momentum (E_T^{miss}) due to the undetected neutrinos and lightest neutralinos. Final states with exactly two hadronically decaying tau leptons ($\tau \rightarrow \text{hadrons } \nu_\tau$) are considered.

The search described in this document uses a dataset of $\sqrt{s} = 13$ TeV pp collisions collected with the ATLAS detector from 2015 to 2018 at the LHC. Similar searches have been performed previously by the ATLAS and CMS Collaborations [19–21]. At LEP [22–26], searches set a lower limit of 86.6 GeV at 95% confidence level (CL) on the mass of promptly decaying staus.

2 ATLAS detector

The ATLAS detector [27] is a multi-purpose particle physics detector with forward-backward symmetric cylindrical geometry and nearly 4π coverage in solid angle.¹ It features an inner tracking detector (ID)

¹ ATLAS uses a right-handed coordinate system with its origin at the nominal interaction point (IP) in the centre of the detector, and the z -axis along the beam line. The x -axis points from the IP to the centre of the LHC ring, and the y -axis points upwards. Cylindrical coordinates (r, ϕ) are used in the transverse plane, ϕ being the azimuthal angle around the z -axis. Observables

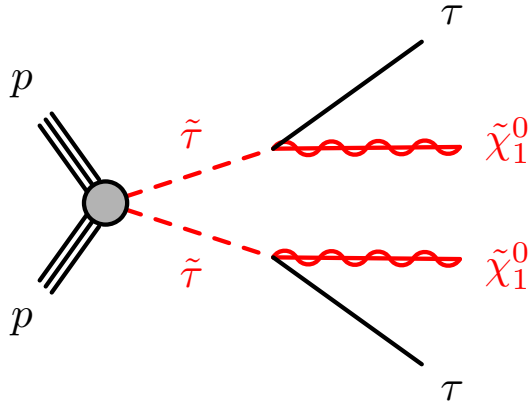


Figure 1: A diagram illustrating the pair production of staus and subsequent decay into a two-tau lepton final state.

surrounded by a 2 T superconducting solenoid, electromagnetic and hadronic calorimeters, and a muon spectrometer (MS). The ID covers the pseudorapidity region $|\eta| < 2.5$ and consists of a silicon pixel detector, a silicon microstrip detector, and a transition radiation tracker. One significant upgrade for the $\sqrt{s} = 13$ TeV running period is the presence of the insertable B-Layer [28], an additional pixel layer close to the interaction point which provides high-resolution hits at a small radius to improve the tracking and vertex reconstruction performance. The calorimeters are composed of high-granularity liquid-argon (LAr) electromagnetic calorimeters with lead, copper, or tungsten absorbers (in the pseudorapidity region $|\eta| < 3.2$) and a steel–scintillator hadronic calorimeter (for $|\eta| < 1.7$). The end-cap and forward regions, spanning $1.5 < |\eta| < 4.9$, are instrumented with LAr calorimeters for both the electromagnetic and hadronic measurements. The MS surrounds the calorimeters and consists of three large superconducting air-core toroidal magnets, each with eight coils, a system of precision tracking chambers ($|\eta| < 2.7$), and detectors for triggering ($|\eta| < 2.4$). A two-level trigger system is used to record events [29].

3 Data and simulated event samples

The analysed dataset, after the application of beam, detector, and data quality requirements, corresponds to an integrated luminosity of 139 fb^{-1} of pp collision data recorded from 2015 to 2018 at $\sqrt{s} = 13$ TeV. The uncertainty on the combined integrated luminosity is 1.7%. It is derived, following a methodology similar to that detailed in [30], from a preliminary calibration of the luminosity scale using $x - y$ beam-separation scans, and using the LUCID-2 detector for the baseline luminosity measurements [31]. The average number of interactions per crossing for this dataset is between 10 and 60, with a mean value of 34.

Monte Carlo (MC) simulated event samples are used to estimate the SUSY signal yields and to aid in evaluating the SM backgrounds. Generated SM events are passed through a detailed detector simulation [32] based on GEANT4 [33]. SUSY MC events are processed using a fast detector simulation that makes use of a parameterised version of the electromagnetic and hadronic calorimeters and full GEANT4 for other detectors. All simulated events are overlaid with multiple pp collisions (pile-up) simulated with the soft strong interaction processes of PYTHIA 8.186 [34] using the A3 set of tuned parameters [35] and the

labelled *transverse* refer to the projection into the x – y plane. The pseudorapidity is defined in terms of the polar angle θ by $\eta = -\ln \tan(\theta/2)$.

NNPDF23LO [36] PDF set. The simulated events are reconstructed using the same algorithms as the data, and are reweighted so that the distribution of the expected number of collisions per bunch crossing matches the one in the data.

3.1 Simulated background samples

Events with $Z/\gamma^* \rightarrow \ell\ell$ ($\ell = e, \mu, \tau$) and $W \rightarrow \ell\nu$ produced with accompanying jets (including light and heavy flavours) were generated at next-to-leading order (NLO) in the strong coupling constant with **SHERPA** 2.2.1 [37, 38]. Matrix elements (ME) were calculated for up to two additional partons at NLO and four additional partons at leading order (LO), using the **Comix** [39] and **OPENLOOPS** [40, 41] generators and merged with the **SHERPA** parton shower (PS) [42] using the ME+PS@NLO prescription [38]. The NNPDF3.0NNLO [43] parton distribution function (PDF) set was used in conjunction with a dedicated PS tuning developed by the **SHERPA** authors. The $W/Z+\text{jets}$ events were normalised using their next-to-next-to-leading order (NNLO) cross sections [44].

Fully leptonically and semileptonically decaying diboson samples ($VV = WW/WZ/ZZ$) are simulated with the **SHERPA** v2.2 [37] generator. In this setup multiple matrix elements are matched and merged with the **SHERPA** parton shower based on Catani-Seymour dipole [39, 42] using the MEPS@NLO prescription [38, 45–47]. The virtual QCD correction for matrix elements at NLO accuracy are provided by the **OPENLOOPS** library [41]. Samples are generated using the NNPDF3.0NNLO set, along with the dedicated set of tuned parton-shower parameters developed by the **SHERPA** authors.

The production of top-quark pairs and single top quarks in the Wt and s -channels was performed with **POWHEG-Box** 2 [48], with the CT10 NLO PDF set in the ME calculations and the ATLAS underlying-event tune A14 [49]. Electroweak t -channel single-top-quark events were generated using the **POWHEG-Box** 1 event generator. The PS, fragmentation, and the underlying event were simulated using **PYTHIA** 8.186 with the CTEQ6L1 [50] PDF set and a corresponding set of A14 tuned parameters. The top-quark mass was set to 172.5 GeV. The cross section was computed at NNLO in α_s , including resummation of next-to-next-to-leading-logarithm (NNLL) soft gluon terms [51] for $t\bar{t}$, to NLO+NNLL accuracy for single-top-quark Wt -channel [52], and to NLO for the t - and s -channels [53]. Top-quark pair production with an additional W or Z boson was performed using **MADGRAPH5_aMC@NLO** 2.2.2 [54], while fragmentation and hadronisation were simulated with **PYTHIA** 8.186. The ATLAS underlying-event tune A14 was used with the NNPDF2.3LO [55] PDF set, and the cross sections were normalised using NLO predictions [56, 57].

Small contributions from Higgs boson production from gluon-gluon fusion and vector boson fusion are modelled using **POWHEG-Box** 2 with the NNPDF3.0NNLO PDF and showered using **PYTHIA** 8.186. Contributions from the associated production of a Higgs boson with a vector boson and from a Higgs boson in association with two top-quarks are simulated using **PYTHIA** 8.186 and **MADGRAPH5_aMC@NLO**, respectively.

For all samples showered with **PYTHIA** 8, **EvtGen** 1.2.0 [58] was used for the simulation of the properties of the bottom and charm hadron decays.

3.2 Simulated signal samples

Simulated signal samples were generated using `MADGRAPH5_aMC@NLO` 2.6.2 interfaced to `PYTHIA` 8.186 with the A14 tune for the PS modelling, hadronisation, and underlying event. The ME calculation is performed at tree level and includes the emission of up to two additional partons. The PDF set used for the generation is NNPDF2.3LO. The ME–PS matching used the CKKW-L [59] prescription, with a matching scale set to one quarter of the mass of the pair of produced particles. Signal cross sections were calculated to next-to-leading order in the strong coupling constant, adding the resummation of soft gluon emission at next-to-leading-logarithm accuracy (NLO+NLL) [60, 61]. The nominal cross section and the uncertainty were taken from an envelope of cross-section predictions using different PDF sets and factorisation and renormalisation scales, as described in Ref. [61–64].

The masses of all charginos and neutralinos apart from the $\tilde{\chi}_1^0$, are set to 2.5 TeV, thus leaving a single kinematically allowed decay: $\tilde{\tau}^\pm \rightarrow \tilde{\chi}_1^0 \tau^\pm$. The left and right staus are combined and have the same mass, which is varied between 100 and 440 GeV and no mixing is assumed between the gauge and mass eigenstates. The mass of the bino-like $\tilde{\chi}_1^0$ is varied in the range 0–200 GeV.

Reference points with $\tilde{\tau}$ masses of 120 GeV, 280 GeV and $\tilde{\chi}_1^0$ mass of 1 GeV are used throughout this note to illustrate typical features of the SUSY models to which this analysis is sensitive. The theoretical cross-section at NLO is 140 (50) fb with $\tilde{\tau}_L \tilde{\tau}_L$ ($\tilde{\tau}_R \tilde{\tau}_R$) of 120 GeV, and 5.8 (2.2) fb with $\tilde{\tau}_L \tilde{\tau}_L$ ($\tilde{\tau}_R \tilde{\tau}_R$) of 280 GeV.

4 Event reconstruction

Events with at least one reconstructed primary vertex [65] are selected. A primary vertex must have at least two associated charged-particle tracks with transverse momentum $p_T > 500$ MeV and be consistent with the collision region. In events with multiple primary vertices, the one with the largest $\sum p_T^2$ of the associated tracks is chosen.

Jets are reconstructed from three-dimensional calorimeter energy clusters [66] using the anti- k_T algorithm [67, 68] with a radius parameter of 0.4. Jet energies are corrected for detector inhomogeneities, the non-compensating response of the calorimeter, and the impact of pile-up, using factors derived from test beam and pp collision data, and from a detailed `GEANT4` detector simulation [69]. The impact of pile-up is accounted for using a technique, based on jet areas, that provides an event-by-event and jet-by-jet correction [70]. Jets that are likely to have originated from pile-up are not considered [71]. The efficiency of this pile-up rejecting selection is approximately 92%. Jets are required to have $p_T > 20$ GeV and $|\eta| < 2.8$. Events containing jets that are likely to have arisen from detector noise or cosmic rays are removed.

Jets containing b -hadrons (b -jets) are identified using the MV2c10 algorithm [72], a multivariate discriminant making use of track impact parameters and reconstructed secondary vertices [73]. Candidate b -jets are required to have $p_T > 20$ GeV and $|\eta| < 2.5$. A working point with an average b -tagging efficiency of 70% for simulated $t\bar{t}$ events is used [74, 75]. This working point corresponds to a c -jet and light-jet rejection of 10 and 200, respectively.

Electron candidates are reconstructed by matching clusters in the electromagnetic calorimeter with charged-particle tracks in the inner detector. Electrons are required to have $p_T > 10$ GeV, $|\eta| < 2.47$, and to

satisfy the ‘loose’ working point according to a likelihood-based identification [76]. Muon candidates are reconstructed from MS tracks matching ID tracks. Muons are required to have $p_T > 10$ GeV and $|\eta| < 2.7$ and fulfil the ‘medium’ quality criteria of Reference [77]. Events containing a muon candidate with a poorly measured charge-to-momentum ratio ($\sigma(q/p) / |q/p| > 0.2$) are rejected.

Electrons and muons are required to satisfy isolation criteria to reduce the number of jets mis-identified as charged leptons. The scalar sum of the p_T of tracks inside a variable-size cone around the lepton (excluding its own track), must be less than 15% of the lepton p_T . The track isolation cone radius² for electrons (muons) ΔR is given by the minimum of $\Delta R = 10$ GeV/ p_T and $\Delta R = 0.2$ (0.3). In addition for electrons (muons) the sum of the transverse energy of the calorimeter energy clusters in a cone of $\Delta R = 0.2$ around the lepton (excluding the energy from the lepton itself) must be less than 20% (30%) of the lepton p_T . For electrons with $p_T > 200$ GeV these isolation requirements are not applied, and instead an upper limit of $\max(0.015 \times p_T \text{ [GeV]}, 3.5 \text{ GeV})$ is placed on the transverse energy of the calorimeter energy clusters in a cone of $\Delta R = 0.2$ around the electron [78].

The efficiencies for electrons and muons to satisfy the reconstruction, identification, and isolation criteria are measured in samples of leptonic Z and J/ψ decays, and corrections are applied to the simulated samples to reproduce the efficiencies in data.

The reconstruction of hadronically decaying tau leptons is based on information from tracking in the ID and three-dimensional clusters of energy in the electromagnetic and hadronic calorimeters. The tau lepton reconstruction algorithm is seeded by jets reconstructed as described above but with $p_T > 10$ GeV and $|\eta| < 2.5$. The reconstructed energies of the hadronically decaying tau lepton candidates are corrected to the tau energy scale, which is calibrated based on simulation and in-situ measurements using $Z \rightarrow \tau\tau$ decays. Tau neutrinos from the hadronic tau lepton decay are not taken into account in the reconstruction and calibration of the tau energy and momentum. Hadronic tau decay candidates are required to have one or three associated charged-particle tracks (prongs) and the total electric charge of those tracks must be ± 1 times the electron charge. To improve the discrimination between hadronically decaying tau leptons and jets a multivariate algorithm is used [79]. The tau lepton identification algorithm is based on a boosted decision tree (BDT) method. The BDT algorithms use various track and cluster variables as input to discriminate tau leptons from jets. For 1-prong (3-prong) tau candidates, the signal efficiencies are 75% (60%) and 60% (45%) for the ‘medium’ and ‘tight’ working points, respectively. In the following, tau lepton candidates are required to satisfy the medium identification criteria for jet discrimination (‘medium’ tau candidates), unless otherwise stated. For electron discrimination, any electron which is overlapping with a 1-prong tau candidate is removed. This requirement has about 95% efficiency, and a rejection factor from 10 to 50 depending on the η range. Tau candidates are required to have $p_T > 20$ GeV and $|\eta| < 2.47$, excluding the transition region between the barrel and end-cap calorimeters ($1.37 < |\eta| < 1.52$).

The simulation is corrected for differences in the efficiencies of the tau identification at both trigger and reconstruction level between data and simulation. For hadronically decaying tau leptons originating from prompt gauge boson decays, the corrections are calculated with a *tag-and-probe* method in a sample of $Z \rightarrow \tau\tau$ events where one tau lepton decays hadronically and the other leptonically into a muon and two neutrinos [80]. Small discrepancies in electron, muon, and jet identification and trigger efficiencies are corrected with scale factors derived in control regions. For the trigger corrections, dedicated regions enriched in $t\bar{t}$, Z and $W+E_T^{\text{miss}}$ were used.

² $\Delta R = \sqrt{(\Delta y)^2 + (\Delta\phi)^2}$, where y is the rapidity and ϕ the azimuthal angle.

The measurement of the missing transverse momentum vector, $\mathbf{p}_T^{\text{miss}}$, and its magnitude, E_T^{miss} , is based on the negative vectorial sum of the \mathbf{p}_T of all identified jets, tau candidates, electrons, muons, and an additional soft term. The soft term is constructed from all high-quality tracks that are associated with the primary vertex but not with any identified particle or jet. In this way, the missing transverse momentum is adjusted for the best calibration of the jets and the other identified particles, while maintaining pile-up independence in the soft term [81].

The possible double counting of reconstructed objects is resolved in the following order. Tau candidates close to electron or muon candidates ($\Delta R < 0.2$) are removed, as are electrons that share a track with a muon. For electrons close to a jet ($\Delta R < 0.4$), the electron is removed, except when $\Delta R < 0.2$ and the jet is not b -tagged, in which case the jet is removed. For a muon close to a jet ($\Delta R < 0.4$), the muon is removed unless the jet has less than three tracks associated to it and is within $\Delta R < 0.2$. In the latter case, the jet is removed. Any remaining jet within $\Delta R = 0.2$ of a tau candidate is removed.

5 Event selection

The events are required to have exactly two medium tau candidates with opposite-sign electric charge (OS) and to have passed either an *asymmetric di-tau* trigger or a combined *di-tau + E_T^{miss}* trigger [82]. In events selected by the *di-tau + E_T^{miss}* trigger, the offline reconstructed E_T^{miss} must be larger than 150 GeV. The trigger efficiency for correctly identified tau leptons is approximately 75 – 80% for events where the tau p_T selection at reconstruction level is for the leading tau candidate $p_T > 95$ (50 – 75) GeV, and the next-to-leading tau candidate $p_T > 60$ – 75 (40) GeV for the *asymmetric di-tau (di-tau + E_T^{miss})* trigger. The higher tau p_T threshold corresponds to the trigger requirement applied in 2018 to cope with the increasing luminosity and the trigger efficiency is nearly constant as a function of the tau p_T and E_T^{miss} . Events with an additional third medium τ or light lepton are rejected.

The reconstructed mass of the two leading tau lepton candidates ($m(\tau_1, \tau_2)$) must be larger than 120 GeV to remove tau leptons originating from decays of low-mass resonances and to suppress contributions from Z +jets and Higgs boson events (Z/H -veto).

To further discriminate the SUSY signal events from SM background processes, additional requirements are applied to define the signal region (SR) selections. To reject events from SM processes containing a top quark, selected events must not contain any b -tagged jets (*b-jet veto*). A lower bound on the *transverse mass* m_{T2} [83, 84] is imposed to reduce contributions from $t\bar{t}$ and WW events. The m_{T2} variable is defined as:

$$m_{T2} = \min_{\mathbf{q}_T} \left[\max \left(m_{T, \tau_1}(\mathbf{p}_{T, \tau_1}, \mathbf{q}_T), m_{T, \tau_2}(\mathbf{p}_{T, \tau_2}, \mathbf{p}_T^{\text{miss}} - \mathbf{q}_T) \right) \right],$$

where \mathbf{p}_{T, τ_1} and \mathbf{p}_{T, τ_2} are the transverse momenta of the two tau candidates, and \mathbf{q}_T is the transverse momentum vector that minimises the larger of the two transverse masses m_{T, τ_1} and m_{T, τ_2} . The latter masses are defined by

$$m_T(\mathbf{p}_T, \mathbf{q}_T) = \sqrt{2(p_T q_T - \mathbf{p}_T \cdot \mathbf{q}_T)}.$$

For $t\bar{t}$ and WW events, in which two W bosons decay leptonically and $\mathbf{p}_T^{\text{miss}}$ is the sum of the transverse momenta of the two neutrinos, the m_{T2} distribution has a kinematic end-point at the W mass. For large mass differences between the staus and the lightest neutralino, the m_{T2} distribution for signal events extends significantly beyond this end-point.

The SRs were optimised for stau discovery by varying the kinematic selection criteria. Events are selected by the asymmetric di-tau trigger to cover the low stau mass region (SR-lowMass) and by the di-tau+ E_T^{miss} trigger to cover the high stau mass region (SR-highMass). $E_T^{\text{miss}} < 150 \text{ GeV}$ ($E_T^{\text{miss}} > 150 \text{ GeV}$) is required for SR-lowMass (SR-highMass) to keep the two SRs orthogonal. Both (at least one) of the tau candidates must satisfy the tight identification criteria for jet discrimination ('tight' tau candidate) for SR-lowMass (SR-highMass). $E_T^{\text{miss}} > 75 \text{ GeV}$ is required for SR-lowMass to increase signal sensitivity. In addition, the two tau candidates are required to satisfy $\Delta R(\tau_1, \tau_2) < 3.2$, $|\Delta\phi(\tau_1, \tau_2)| > 0.8$ and $m_{\text{T2}} > 70 \text{ GeV}$ in order to suppress additional contributions from SM backgrounds. The requirements for the SRs are summarised in Table 1.

Table 1: Summary of selection requirements for the signal regions.

SR-lowMass	SR-highMass
2 tight τ s (OS) asymmetric di-tau trigger $75 < E_T^{\text{miss}} < 150 \text{ GeV}$ tau p_T and E_T^{miss} cuts described in Section 5 light lepton veto and 3rd medium τ veto b -jet veto Z/H veto ($m(\tau_1, \tau_2) > 120 \text{ GeV}$) $\Delta R(\tau_1, \tau_2) < 3.2$ $ \Delta\phi(\tau_1, \tau_2) > 0.8$ $m_{\text{T2}} > 70 \text{ GeV}$	2 medium τ s (OS), ≥ 1 tight τ di-tau+ E_T^{miss} trigger $E_T^{\text{miss}} > 150 \text{ GeV}$

6 Standard Model background estimation

The main SM processes contributing to the selected final states are multi-jet, W +jets and diboson production. Background events may contain a combination of 'real' tau leptons, defined as correctly identified prompt tau leptons, or 'fake' tau leptons, which can originate from a misidentified quark or gluon jet, an electron, or a muon.

In multi-jet events in the SRs, nearly all tau candidates are misidentified jets. The multi-jet contribution in the SRs is estimated from data, as described in Section 6.1. The contribution arising from heavy-flavour multi-jet events containing a real tau lepton from the heavy-flavour quark decay is included in the multi-jet estimation. The contribution of W +jets events, which contain one real tau lepton from the W decay and one or more misidentified jets, is estimated from MC simulation and normalised to data in a dedicated control region (CR), as described in Section 6.2.

Diboson production contributes mainly events containing real tau leptons originating from WW and ZZ decaying into $\tau\tau\nu\nu$ final state. Additional SM backgrounds arise from Z +jets production, or events that contain a top quark or a top-quark pair in association with jets or additional W or Z bosons (collectively referred to as *top* quark background in the following). The contribution from real tau leptons exceeds 90% in Z +jets and diboson production, and ranges from 45% to 75% in backgrounds containing top quarks according to the MC simulation. The contribution of fake tau leptons from heavy-flavour decays in jets is found to be negligible in MC simulation. To estimate the irreducible background, which includes diboson, Z +jets and top quark events, only MC simulated samples are used and validated in dedicated validation regions (VRs), as described in Section 6.3.

A simultaneous fit of the event yields in the control regions based on the profile likelihood method [85] is performed to normalise the multi-jet and W +jets background estimates and propagate systematic uncertainties, as described in Section 8. The sources of systematic uncertainty in the background estimates are described in Section 7. Results showing the agreement in the validation regions after the fit are labeled “post-fit” and results shown in the control regions prior to the fit are labeled “pre-fit”.

6.1 Multi-jet background estimation

One of the dominant backgrounds in the SRs originates from jets misidentified as tau leptons in multi-jet production. It accounts for 44% (30%) of the total SM contribution in SR-lowMass (SR-highMass). This contribution is estimated from data using the so-called *ABCD* method. All regions used for the *ABCD* method are schematically drawn in Figure 2. Four exclusive regions, labelled as A, B, C, and D, are defined in a two-dimensional plane as a function of two (or more) discriminating variables that are largely uncorrelated. The ratio of events in the regions C and B is then equal to that in the regions D and A. The number of multi-jet events in region D, N_D , can therefore be calculated from the multi-jet events in region A, N_A , multiplied by the transfer factor $T = N_C/N_B$, where N_C (N_B) is the number of multi-jet events in region C (B). The region D corresponds to the SR defined in Section 5, whereas the regions A, B, and C are control regions defined accordingly. In the following, the regions A, B, C, D are labelled as CR-A, CR-B, CR-C and SR-lowMass (or SR-highMass), respectively. The *ABCD* method only provides a first level estimate of multi-jet background, the normalization and uncertainty being then modified by a combined fit to CR-A (lowMass) and CR-A (highMass) described in Section 8 while the transfer factor is fixed.

The definition of the regions used in the *ABCD* method for the multi-jet estimation is given in Table 2; only those requirements that are different in the CRs/VRs with respect to the SRs are listed. In all of the regions, the *di-tau + E_T^{miss}* or *asymmetric di-tau* triggers described in Section 5 are used. CR-A and CR-B include events with two loose taus, either same sign (SS) or OS, and veto events with two medium OS taus to remain orthogonal to the SR and reduce the potential signal contamination. CR-C and CR-B have events with lower m_{T2} and E_T^{miss} values and no $\Delta R(\tau_1, \tau_2)$ cut. Furthermore, two sets of VRs, VR-E and VR-F, are defined corresponding to each SR. The validation regions are used to verify the extrapolation of the *ABCD* estimation to the SRs and to estimate the systematic uncertainty from the residual correlation between the tau lepton identification and charge requirements and the kinematic variables m_{T2} .

The number of multi-jet events in the control and validation regions is estimated from data after subtraction of other SM contributions estimated from MC simulation. In CR-B and VR-E, around 96% and 90% (75% and 79%) of the events are from multi-jet production in the lowMass (highMass) regions, respectively. For CR-A and CR-C the multi-jet purity is 74% and 57% (58% and 53%) in the lowMass (highMass) regions, respectively. In VR-F the multi-jet purity is 51%. Good agreement between data and the estimated SM background is found for the m_{T2} and E_T^{miss} distributions in the validation regions, as shown in Figure 3.

The signal contamination in multi-jet CR-A is defined as the ratio of the number of signal events to the sum of the number of signal events and SM background processes. The signal contamination in CR-A for the SR ranges from 0.4% (2.2%) up to 9.4% (21.4%) for SR-lowMass (SR-highMass). This is taken into account in the fit for signal hypothesis testing in Section 10, and the effect on limits is small.

The multi-jet background estimation is also validated using a different method, the *fake-factor method*. Fake factors (FF) are derived for each of the two tau candidates with the same electric charge in a multi-jet enriched region. They are computed as the ratio of the number of leading or subleading tau candidates passing all of the nominal signal identification criteria over the number of tau candidates failing the

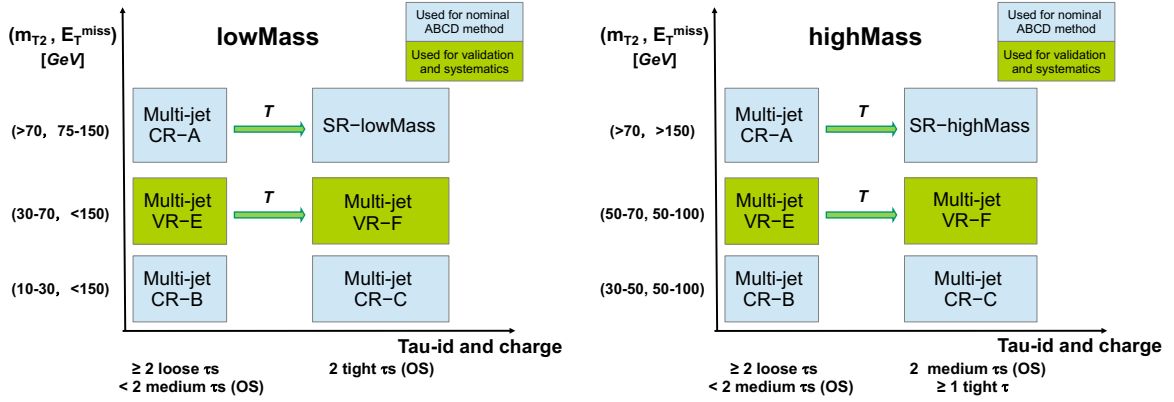


Figure 2: Illustration of the ABCD method for the multi-jet background determination for SR-lowMass (left) and SR-highMass (right). The control regions A, B, C, and signal region D for the ABCD method described in the text (labelled as CR-A, CR-B, CR-C and SR-lowMass/SR-highMass) are drawn as light blue boxes. Shown in green and labelled as VR are the regions E and F, which are used to validate the ABCD method and to estimate the systematic uncertainty.

Table 2: Definition of the regions used in the ABCD method for the multi-jet estimation in the SRs. Only those requirements that are different in the CRs/VRs with respect to the SRs are listed.

CR - A (lowMass)	SR - lowMass	CR - A (highMass)	SR - highMass
≥ 2 loose τ s	2 tight τ s (OS)	≥ 2 loose τ s	2 medium τ s (OS)
< 2 medium τ s (OS)	–	< 2 medium τ s (OS)	≥ 1 tight τ
$\Delta R(\tau_1, \tau_2) < 3.2$	$\Delta R(\tau_1, \tau_2) < 3.2$	$E_T^{\text{miss}} > 150$ GeV	$E_T^{\text{miss}} > 150$ GeV
$75 < E_T^{\text{miss}} < 150$ GeV	$75 < E_T^{\text{miss}} < 150$ GeV	$\Delta R(\tau_1, \tau_2) < 3.2$	$\Delta R(\tau_1, \tau_2) < 3.2$
$m_{T2} > 70$ GeV			
VR - E (lowMass)	VR - F (lowMass)	VR - E (highMass)	VR - F (highMass)
≥ 2 loose τ s	2 tight τ s (OS)	≥ 2 loose τ s	2 medium τ s (OS)
< 2 medium τ s (OS)	–	< 2 medium τ s (OS)	≥ 1 tight τ
$\Delta R(\tau_1, \tau_2) < 3.2$	$\Delta R(\tau_1, \tau_2) < 3.2$	$50 < E_T^{\text{miss}} < 100$ GeV	$50 < E_T^{\text{miss}} < 100$ GeV
$E_T^{\text{miss}} < 150$ GeV	$E_T^{\text{miss}} < 150$ GeV	$\Delta R(\tau_1, \tau_2) < 3.2$	$\Delta R(\tau_1, \tau_2) < 3.2$
$30 < m_{T2} < 70$ GeV	$30 < m_{T2} < 70$ GeV	$50 < m_{T2} < 70$ GeV	$50 < m_{T2} < 70$ GeV
CR - B (lowMass)	CR - C (lowMass)	CR - B (highMass)	CR - C (highMass)
≥ 2 loose τ s	2 tight τ s (OS)	≥ 2 loose τ s	2 medium τ s (OS)
< 2 medium τ s (OS)	–	< 2 medium τ s (OS)	≥ 1 tight τ
no $\Delta R(\tau_1, \tau_2)$ cut			
$E_T^{\text{miss}} < 150$ GeV	$E_T^{\text{miss}} < 150$ GeV	$50 < E_T^{\text{miss}} < 100$ GeV	$50 < E_T^{\text{miss}} < 100$ GeV
$10 < m_{T2} < 30$ GeV	$10 < m_{T2} < 30$ GeV	$30 < m_{T2} < 50$ GeV	$30 < m_{T2} < 50$ GeV

requirement on the jet-veto BDT, and are parameterized with respect to the p_T , η and N_{prong} of the tau candidates. An observed dependence on the BDT output score of the second tau candidate in the event is also taken into account. The expected number of multi-jet events entering a selection is computed by applying the fake factors to the yields in a set of sideband regions where either the leading, subleading or both tau candidates fail the identification requirements. Agreement of the predicted multi-jet event yields from the ABCD method and the FF method in both SRs and the multi-jet VRs is observed within the statistical and systematic uncertainties.

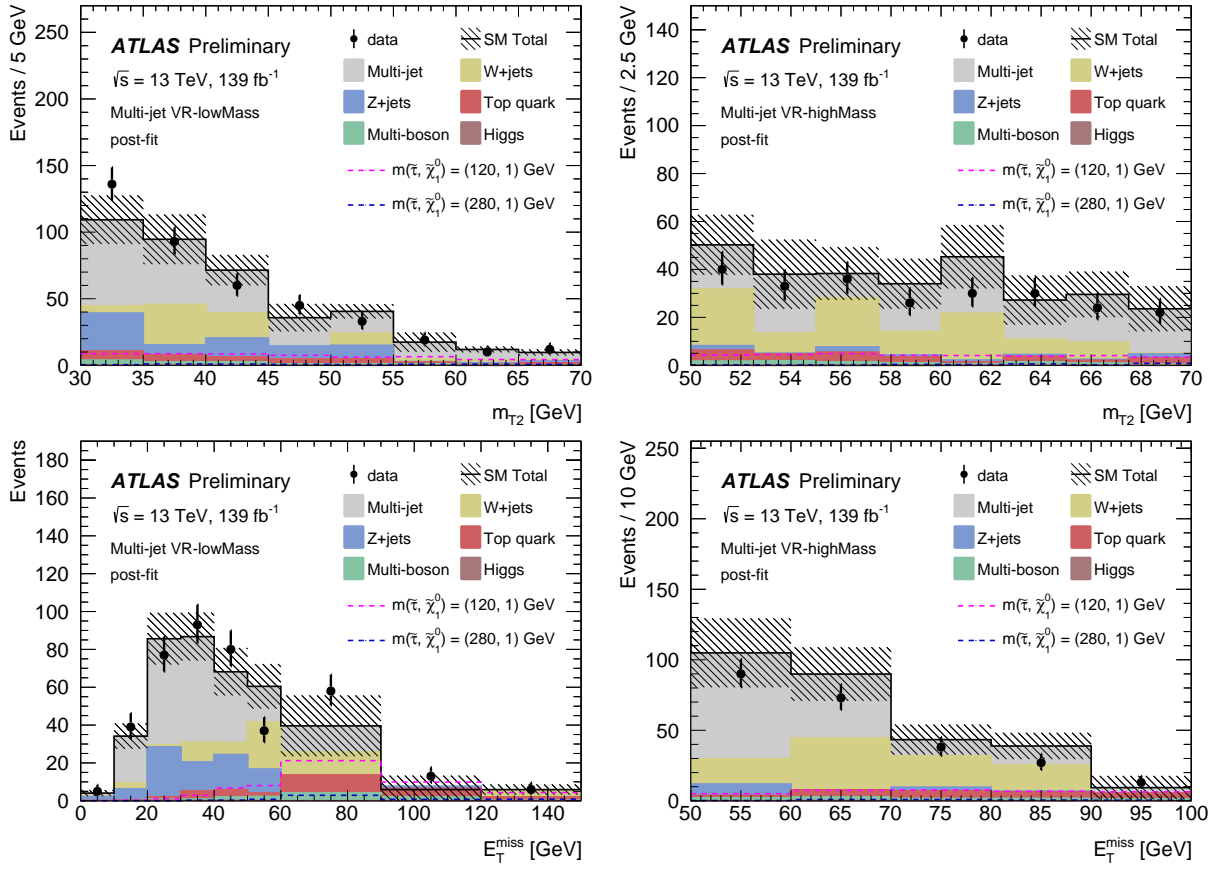


Figure 3: The m_{T2} (top) and E_T^{miss} (bottom) post-fit distributions in the multi-jet background validation region VR-F (lowMass) at left and VR-F (highMass) at right. The stacked histograms show the contribution of each relevant SM process. The multi-jet shape is taken from VR-E in the *ABCD* method and the normalization is determined by the transfer factor T and rescaled by a correction factor determined by the fit. The hatched bands represent the combined statistical and systematic uncertainties in the sum of the SM backgrounds shown. For illustration, the distributions of the SUSY reference points (defined in Section 3) are also shown as dashed lines.

6.2 $W+\text{jets}$ background estimation

The production of $W+\text{jets}$ events with at least one misidentified tau lepton is an important background, accounting for about 25% of the expected SM background in the two SRs. A dedicated control region ($W\text{-CR}$) is used to normalise the $W+\text{jets}$ MC estimate to data and another region is used to validate the $W+\text{jets}$ estimate (W validation region, $W\text{-VR}$). To suppress multi-jet contamination, the $W\text{-CR}$ is enriched in events where the W boson decays leptonically into a muon and a neutrino. Events are selected with a single-muon trigger using the lowest unprescaled p_T thresholds available. Events containing exactly one muon and one candidate tau with opposite electric charge are selected. The muon is required to have $p_T > 50$ GeV. The tau candidate must satisfy the medium tau lepton identification criteria and is required to have $p_T > 60$ GeV.

The contribution from events with top quarks is suppressed by rejecting events containing b -tagged jets, and rejecting events which are kinematically compatible with $t\bar{t}$ production (top-tagged) through the use of the *contransverse mass* variable m_{CT} [86]. The definitions of the $W\text{-CR}$ and $W\text{-VR}$ are given in Table 3.

The transverse mass of the $\mu + E_T^{\text{miss}}$ system, $m_{T,\mu}$ is used to reduce the contribution from Z +jets, top-quark and diboson contributions. To further suppress multi-jet and Z +jets events, E_T^{miss} and $\Delta R(\tau, \mu)$ cuts are applied. The invariant mass of the muon and tau lepton, $m(\mu, \tau)$, and $m_{T,\tau} + m_{T,\mu}$ are used to improve the W +jets purity. Events in the W -CR (W -VR) are selected by requiring low (high) m_{T2} .

Table 3: Summary of selection requirements for the W control (W -CR) and validation (W -VR) regions.

W -CR	W -VR
1 medium τ and 1 isolated μ (OS)	
single-muon trigger	
$p_T(\tau) > 60 \text{ GeV}$, $p_T(\mu) > 50 \text{ GeV}$	
$E_T^{\text{miss}} > 60 \text{ GeV}$	
b -jet veto and top-tagged events veto	
$m(\mu, \tau) > 70 \text{ GeV}$	
$1 < \Delta R(\mu, \tau) < 3.5$	
$50 < m_{T,\mu} < 150 \text{ GeV}$	
$m_{T,\mu} + m_{T,\tau} > 250 \text{ GeV}$	
$30 < m_{T2} < 70 \text{ GeV}$	$ m_{T2} > 70 \text{ GeV}$

The multi-jet contribution in the W -CR (W -VR) is estimated using the so-called *OS*–*SS* method by counting the number of events in data satisfying the same requirements as the W -CR (W -VR) but with the electric charge of the two leptons having the same sign. Events from SM processes other than multi-jet production are subtracted from the data counts in the *SS* region using MC simulation. The *OS*–*SS* method relies on the fact that in the multi-jet background the ratio of *SS* to *OS* events is close to unity, while it is around 7 for W +jets production. The latter is dominated by gu/gd -initiated processes that often give rise to a jet originating from a quark, the charge of which is anti-correlated with the W boson charge. Based on studies with simulated samples, a systematic uncertainty of 100% is assigned to the multi-jet estimate in the W -CR.

The purity of the selection in W +jets events is around 79% (69%) in the W -CR (W -VR). The m_{T2} distributions in the W -CR and W -VR are shown in Figure 4, and a good agreement, both for the normalization and shape, between data and SM predictions is observed. The signal contamination in the W -CR and W -VR is negligible. The theory uncertainties on the W +jets estimation in the W -CR and W -VR are considered uncorrelated, and thus in this case, the full uncertainty on the W +jets estimate is applied to the W -VR.

6.3 Irreducible background estimation

Irreducible SM backgrounds arise mainly from $t\bar{t}$, single top quark, $t\bar{t}+V$, Z +jets, and multi-boson (diboson (WW , WZ and ZZ), triboson (VVV)) and Higgs processes. They are estimated with MC simulation. Other SM backgrounds are found to be negligible.

The inclusive contribution from $t\bar{t}$, single top, $t\bar{t}+V$ and Z +jets amounts to about 8% and 20% of the total background in SR-lowMass and SR-highMass, respectively. The diboson background accounts for 23 – 25% of the total SM contribution in the SRs and mainly arises from $WW \rightarrow \tau\nu\tau\nu$ and $ZZ \rightarrow \tau\tau\nu\nu$ events, in which more than 96% of the contribution is from events with two real tau leptons according to the MC simulation.

The MC estimates are validated in regions enriched in Z +jets, top-quark and multi-boson events. For these validation regions, events are required to pass either the combined di-tau + E_T^{miss} trigger or the asymmetric

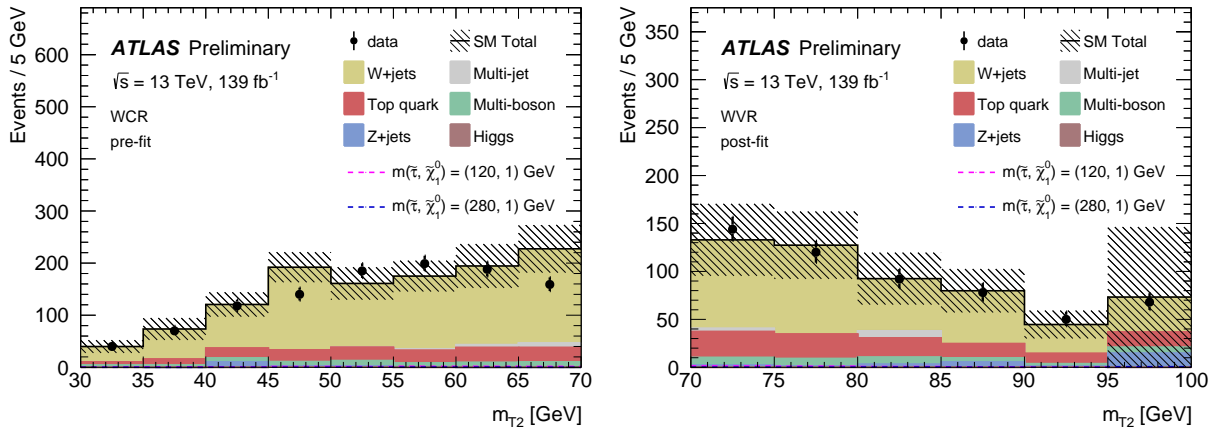


Figure 4: The pre-fit and post-fit m_{T2} distributions in the W -CR (left) and W -VR (right) regions, respectively. The SM backgrounds other than multi-jet production are estimated from MC simulation. The multi-jet contribution is estimated from data using the *OS-SS* method. The hatched bands represent the combined statistical and systematic uncertainties of the total SM background. For illustration, the distributions of the SUSY reference points defined in Section 3 are also shown as dashed lines. The last bin of the right plot includes the overflow events.

di-tau trigger with the same offline threshold cut as described in Table 4. Events are required to have at least two tau candidates satisfying the medium tau lepton identification criteria with opposite electric charge, and at least one tau candidate must satisfy the tight tau lepton identification criteria to be close to the SRs. In the top-quark validation regions (TVR), to increase the contribution from top-quark events, events must contain at least one b -tagged jet with $p_T > 20$ GeV and $\Delta R(\tau_1, \tau_2) > 1.2$. In order to be close to the SRs, $m_{T2} > 60$ GeV is required. In the Z -jets and multi-boson validation regions (ZVR , $VVVR$), in order to suppress top-quark backgrounds, events containing b -tagged jets are vetoed. To further enhance the purity of Z -jets events, $\Delta R(\tau_1, \tau_2)$, $m(\tau_1, \tau_2)$ and m_{T2} requirements are applied. Further, $m(\tau_1, \tau_2)$, $m_{T, \tau_1} + m_{T, \tau_2}$ and m_{T2} cuts are required to enhance multi-boson purity. The $ZVRs$, $TVRs$ and $VVVRs$ requirements are summarised in Table 4.

The event yields of data and SM predictions in the top quark (TVR), Z -jets (ZVR) and multi-boson ($VVVR$) validation regions are shown in Figure 5. Good agreement between data and the SM prediction is observed in all validation regions within uncertainty. The purity of the selection in Z -jets and $t\bar{t}$ (multi-boson) events is around 86 – 96% (47 – 71%) in the respective validation regions.

7 Systematic uncertainties

Systematic uncertainties have an impact on the estimates of the background and signal event yields in the control and signal regions. Uncertainties arising from experimental and theoretical sources are estimated.

The main sources of experimental systematic uncertainty in the SM background estimates include tau lepton and jet energy scale and resolution, tau lepton identification, pile-up, and uncertainties related to the modelling of E_T^{miss} in the simulation. The uncertainties in the energy and momentum scale of each of the objects entering the E_T^{miss} calculation are estimated, as well as the uncertainties in the soft-term resolution and scale. A variation in the pile-up reweighting of the MC simulated event samples is included to cover modelling uncertainties [87]. The main contributions to experimental systematic uncertainties in the SRs

Table 4: Summary of selection requirements for top quark (TVR), Z +jets (ZVR) and multi-boson (VVVR) validation regions.

Selections	TVR -lowMass	ZVR -lowMass	VVVR -lowMass	TVR -highMass	ZVR -highMass	VVVR -highMass
$m(\tau_1, \tau_2)$	≥ 1 b -jet			≥ 1 b -jet		
$\Delta R(\tau_1, \tau_2)$	–	< 70 GeV	< 110 GeV	–	< 60 GeV	< 110 GeV
$m_{T, \tau_1} + m_{T, \tau_2}$	> 1.2	< 1	–	> 1.2	< 1	–
m_{T2}	–	–	> 250 GeV	–	–	> 200 GeV
Trigger	> 60 GeV	< 60 GeV	> 60 GeV	> 60 GeV	< 60 GeV	> 60 GeV
	≥ 2 medium τ s (OS), ≥ 1 tight τ			b -jet veto		
	b -jet veto			b -jet veto		
	asymmetric di- τ trigger			di- τ + E_T^{miss} trigger		
	$60 < E_T^{\text{miss}} < 150$ GeV			$E_T^{\text{miss}} > 150$ GeV		
	τ p_T and E_T^{miss} cuts described in Section 5					

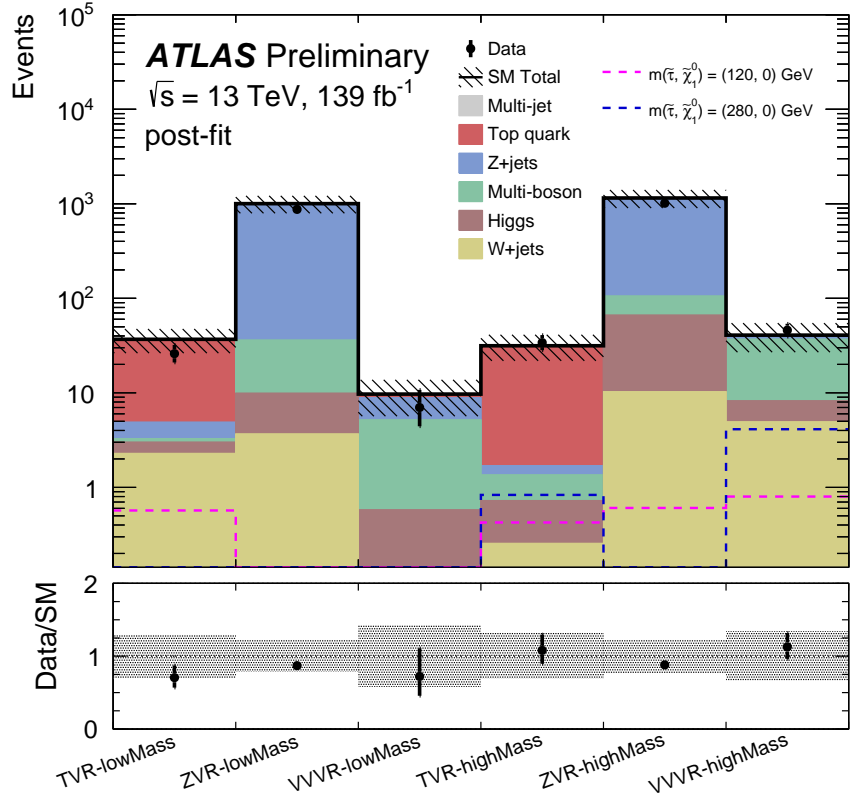


Figure 5: The post-fit yields in the TVRs, ZVRs and VVVRs. The SM backgrounds other than multi-jet production are estimated from MC simulation. The multi-jet contribution is negligible and is estimated from data using the ABCD method, using CRs obtained with the same technique used for the SRs, and described in Section 6.1. The hatched bands represent the combined statistical and systematic uncertainties of the total SM background. For illustration, the distributions of the SUSY reference points (defined in Section 3) are also shown as dashed lines. The lower panels show the ratio of data to the SM background estimate.

are from the tau lepton identification and energy scale [79], and jet energy scale and resolution. Other contributions are less than 3%.

Theoretical uncertainties affecting the `SHERPA` MC event generator predictions, for the W +jets, Z +jets and multi-boson samples, are estimated by varying the renormalisation and factorisation scale as well as PDF uncertainties following the PDF4LHC recommendations [88]. The theory uncertainty in W +jets (multi-boson) production is mainly from the QCD renormalisation scale, which amounts to 5 – 8% (5 – 6%).

The following sources of uncertainty are considered for the ABCD method used to determine the multi-jet background: the correlation between the tau identification, the charge requirement, and the kinematic variables m_{T2} , the limited number of events in the CRs, and the subtraction of other SM backgrounds. The systematic uncertainty in the correlation is estimated by comparing the transfer factor from CR-B to CR-C to that of VR-E to VR-F. The experimental systematic and theory uncertainty in the non-multi-jet background subtraction in the control regions is estimated by considering the systematic uncertainty of the MC estimates of the non-multi-jet background in these regions. These uncertainties are negligible due to high multi-jet purity in the CRs. The statistical uncertainty of the event yields in the control regions is propagated to the signal regions as a systematic uncertainty.

The systematic uncertainties on the background estimates in the SRs are summarised in Table 5. The dominant uncertainties in the SRs are the statistical uncertainty of the MC predictions (11 – 21%), tau identification and energy scale (10 – 19%), and multi-jet background normalisation (9 – 13%).

The total uncertainty in the signal yields for the SUSY reference points defined in Section 3 is about 18 – 31%. The dominant uncertainties in the SRs are tau identification and energy scale (14 – 29%) and the statistical uncertainty of the signal MC predictions (6 – 10%). The cross-section uncertainty is taken into account as main source of signal modeling theoretical uncertainty, and it varies from 3% to 7% for the considered SUSY models.

8 Statistical analysis

The statistical interpretation of the results is performed using the profile likelihood method implemented in the `HistFitter` framework [89]. The likelihood function is a product of the probability density functions, one for each region contributing to the fit. The number of events in a given CR or SR is described using a Poisson distribution, the mean of which is the sum of the expected contributions from all background and signal sources. The systematic uncertainties in the expected event yields are included as nuisance parameters and are assumed to follow a Gaussian distribution with a width determined from the size of the uncertainty. Correlations between control and signal regions, and between background processes are taken into account with common nuisance parameters. The fit parameters are determined by maximising the product of the Poisson probability functions and the constraints for the nuisance parameters.

Three types of fits are performed for the combined SR-lowMass and SR-highMass.

- The *background-only* fit uses as input the number of observed events and other SM contributions in the multi-jet CR-A and W -CR as well as the transfer factors, which relate the number of multi-jet or W +jets events from control regions to signal regions. The free parameters in the fit are the normalisations of the W +jets and multi-jet contributions. The signal is assumed to be absent in this fit.

- A *model-independent limit* fit combines the data event yield in a given SR with the SM background estimate and its uncertainties to test whether any non-SM signal contributes to the SR. The significance of a possible excess of observed events over the SM prediction is quantified by the one-sided probability, $p(\text{signal} = 0)$ denoted by p_0 , of the background alone to fluctuate to the observed number of events or higher using the asymptotic formula described in Ref. [85]. The background yields and uncertainties are taken from the *background-only* fit results. The presence of a non-SM signal would manifest itself in a small p_0 value.
- In the *model-dependent limit* fit the SUSY signal is allowed to populate both the signal and the control regions, and it is scaled by a freely floating signal normalisation factor. The background normalisation factors are also determined simultaneously in the fit. A SUSY model with a specific set of sparticle masses is rejected if the upper limit at 95% confidence level (CL) of the signal normalisation factor obtained in this fit is smaller than unity.

9 Results

The observed number of events in each control, validation, and signal region and the expected contributions from SM processes are given in Table 6. The contributions of multi-jet and W +jets events are scaled with the normalisation factors obtained from the background-only fit described in Section 8. The multi-jet normalisation with respect to the prediction from the ABCD method in the SR is 1.03 and has an uncertainty of around 30%, due to the small number of observed events in the multi-jet CR-A. The W +jets normalisation

Table 5: The relative systematic uncertainty (%) in the background estimate (signal reference points) in the SR-lowMass and SR-highMass from the leading sources at top (bottom). Uncertainties from different sources in the background estimate may be correlated, and do not necessarily add in quadrature to the total uncertainty.

Source of systematic uncertainty	SR-lowMass (%)	SR-highMass (%)
Statistical uncertainty of MC samples	11	21
Tau identification and energy scale	19	10
Normalisation uncertainties of the multi-jet background	13	9
Multi-jet estimation	6	11
W +jets theory uncertainty	5	8
Diboson theory uncertainty	5	6
Jet energy scale and resolution	5	8
E_T^{miss} soft-term resolution and scale	2	2
Total	28	33
Source of systematic uncertainty	SR-lowMass (%)	SR-highMass (%)
$m(\tilde{\tau}, \tilde{\chi}_1^0)$ GeV	(120, 1)	(280, 1)
Tau identification and energy scale	29	14
Statistical uncertainty of MC samples	6	10
Signal cross section uncertainty	4	6
Jet energy scale and resolution	3	2
E_T^{miss} soft-term resolution and scale	3	< 1
Total	31	18

is 0.91 ± 0.11 . The m_{T2} distributions are shown in Figure 6 for data, expected SM backgrounds, and the SUSY reference points defined in Section 3. In both signal regions, observations and background predictions are found to be compatible within uncertainties.

Expected event yields for the SUSY reference points as well as the one-sided p_0 -values and the observed and expected 95% CL, derived from the individual model-independent fits of SR-lowMass and SR-highMass, are shown in Table 7. All limits are calculated using the CL_s prescription [90]. Normalising these by the integrated luminosity of the data sample, they can be interpreted as upper limits on the visible non-SM cross section, σ_{vis}^{95} , which is defined as the product of acceptance, reconstruction efficiency and production cross section.

Table 6: Observed and expected numbers of events in the control, validation, and signal regions. The expected event yields of SM processes are given after the background-only fit described in Section 8. The entries marked as “–” are negligible. The uncertainties correspond to the sum in quadrature of statistical and systematic uncertainties. The correlation of systematic uncertainties among control regions and among background processes is fully taken into account.

SM process	Multi-jet CR	Multi-jet CR	W-CR	W-VR	SR	SR
	-lowMass	-highMass			-lowMass	
Diboson	1.4 ± 0.6	1.9 ± 1.0	63 ± 18	37 ± 11	1.4 ± 0.8	2.6 ± 1.2
W +jets	13 ± 5	4^{+7}_{-4}	850 ± 70	370 ± 120	1.5 ± 0.7	2.5 ± 1.9
Top quark	2.7 ± 0.9	3.3 ± 1.6	170 ± 40	114 ± 31	$0.04^{+0.80}_{-0.04}$	2.0 ± 0.5
Z +jets	$0.3^{+1.4}_{-0.3}$	1.5 ± 0.7	13 ± 7	27 ± 20	$0.4^{+0.5}_{-0.4}$	$0.04^{+0.13}_{-0.04}$
Higgs	$0.01^{+0.33}_{-0.01}$	0.01 ± 0.01	$1.1^{+1.8}_{-1.1}$	$0.5^{+1.0}_{-0.5}$	$0.01^{+0.02}_{-0.01}$	–
Multi-jet	55 ± 10	16 ± 7	3.1 ± 3.1	–	2.6 ± 0.7	3.1 ± 1.5
SM total	72 ± 8	27 ± 5	1099 ± 33	540 ± 130	6.0 ± 1.7	10.2 ± 3.3
Observed	72	27	1099	552	10	7

Table 7: Expected event yields for the SUSY reference points (defined in Section 3) are shown along with the one-sided p_0 -values, and the observed and expected 95% CL upper limits on the visible non-SM cross section (σ_{vis}^{95}) are given. Values of $p_0 > 0.5$ are truncated to $p_0 = 0.5$.

	SR-lowMass	SR-highMass
$m(\tilde{\tau}, \tilde{\chi}_1^0) = (120, 1) \text{ GeV}$	9.8 ± 3.1	7.2 ± 2.2
$m(\tilde{\tau}, \tilde{\chi}_1^0) = (280, 1) \text{ GeV}$	5.9 ± 1.5	14.0 ± 2.5
p_0	0.11	0.50
Expected $\sigma_{\text{vis}}^{95} \text{ [fb]}$	$0.055^{+0.025}_{-0.014}$	$0.065^{+0.025}_{-0.019}$
Observed $\sigma_{\text{vis}}^{95} \text{ [fb]}$	0.08	0.05

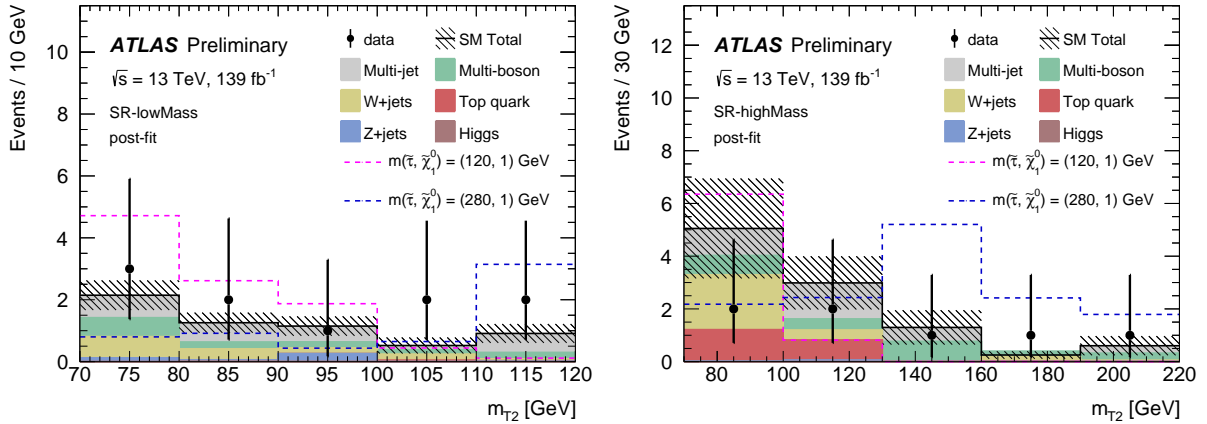


Figure 6: The post-fit m_{T2} distribution for SR-lowMass (left) and SR-highMass (right). The stacked histograms show the expected SM backgrounds. The multi-jet contribution is estimated from data using the ABCD method. The contributions of multi-jet and W -jets events are scaled with the corresponding normalisation factors. The hatched bands represent the sum in quadrature of systematic and statistical uncertainties of the total SM background. For illustration, the distributions of the SUSY reference points (defined in Section 3) are also shown as dashed lines. The last bin includes the overflow events.

10 Interpretation

In the absence of a significant excess over the expected SM background, the observed and expected numbers of events in the signal regions are used to place exclusion limits at 95% CL using the model-dependent limit fit. The exclusion limits for the combined SR-lowMass and SR-highMass for the simplified models described in Section 3 are shown in Figure 7. The solid (dashed) lines show the observed (expected) exclusion contours. The band around the expected limit shows the $\pm 1\sigma$ variations, including all uncertainties except theoretical uncertainties in the signal cross section. The dotted lines around the observed limit indicate the sensitivity to $\pm 1\sigma$ variations of the theoretical uncertainties in the signal cross section. While the left-handed stau pair production has a higher production cross section, the right-handed stau pair production has a higher efficiency times acceptance due to kinematic differences in the resulting decay products.

Stau masses from 120 GeV to 390 GeV are excluded for a massless lightest neutralino in the scenario of the combined left- and right-handed $\tilde{\tau}_{R,L}^+ \tilde{\tau}_{R,L}^-$ production. For the left-handed production only, $\tilde{\tau}_L^+ \tilde{\tau}_L^-$, the exclusion extends from 160 GeV to 300 GeV.

These limits significantly extend previous results [19–21] in the high $\tilde{\tau}$ mass region.

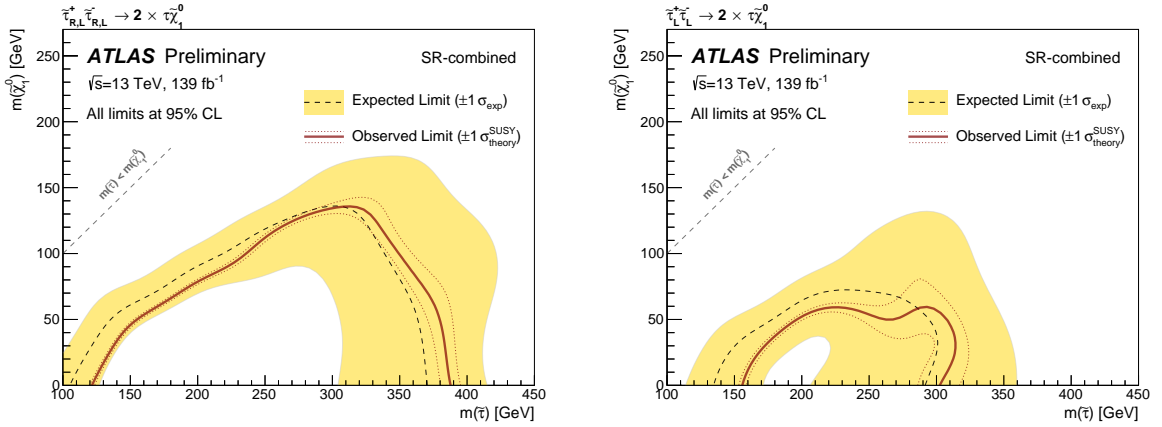


Figure 7: The 95% CL exclusion contours for the combined fit of SR-lowMass and SR-highMass for simplified models with (a) combined $\tilde{\tau}_{R,L}^+ \tilde{\tau}_{R,L}^- \rightarrow 2 \times \tilde{\tau} \chi_1^0$ production and (b) $\tilde{\tau}_L^+ \tilde{\tau}_L^- \rightarrow 2 \times \tilde{\tau} \chi_1^0$ only production. The text provides details of exclusion curves and uncertainty bands.

11 Conclusion

Searches for stau-pair ($\tilde{\tau}\tilde{\tau}$) production of supersymmetric particles in events with at least two hadronically decaying tau leptons are performed using 139 fb^{-1} of pp collision data at $\sqrt{s} = 13 \text{ TeV}$ recorded with the ATLAS detector at the LHC. Agreement between data and SM predictions is observed in two optimised signal regions. The results are used to set limits on the visible cross section for events beyond the Standard Model in each signal region.

Exclusion limits are placed on parameters of simplified electroweak supersymmetry models in scenarios of $\tilde{\tau}\tilde{\tau}$ production. $\tilde{\tau}$ masses from 120 GeV to 390 GeV are excluded for a massless lightest neutralino in the scenario of direct production of stau pairs, with each stau decaying into the lightest neutralino and one tau lepton. These limits significantly extend previous results by ATLAS and CMS experiments in the high $\tilde{\tau}$ mass region.

Acknowledgements

We honour the memory of our colleague Jihyun Jeong, who died shortly before the completion of this work.

References

- [1] Yu. A. Golfand and E. P. Likhtman, *Extension of the Algebra of Poincare Group Generators and Violation of p Invariance*, JETP Lett. **13** (1971) 323, [Pisma Zh. Eksp. Teor. Fiz. 13 (1971) 452].
- [2] D. V. Volkov and V. P. Akulov, *Is the Neutrino a Goldstone Particle?*, Phys. Lett. B **46** (1973) 109.
- [3] J. Wess and B. Zumino, *Supergauge Transformations in Four-Dimensions*, Nucl. Phys. B **70** (1974) 39.

- [4] J. Wess and B. Zumino, *Supergauge Invariant Extension of Quantum Electrodynamics*, *Nucl. Phys. B* **78** (1974) 1.
- [5] S. Ferrara and B. Zumino, *Supergauge Invariant Yang-Mills Theories*, *Nucl. Phys. B* **79** (1974) 413.
- [6] A. Salam and J. A. Strathdee, *Supersymmetry and Nonabelian Gauges*, *Phys. Lett. B* **51** (1974) 353.
- [7] S. P. Martin, *A Supersymmetry primer*, *Adv. Ser. Direct. High Energy Phys.* **18** (1998) 1, [arXiv:hep-ph/9709356](https://arxiv.org/abs/hep-ph/9709356).
- [8] G. R. Farrar and P. Fayet, *Phenomenology of the Production, Decay, and Detection of New Hadronic States Associated with Supersymmetry*, *Phys. Lett. B* **76** (1978) 575.
- [9] H. Goldberg, *Constraint on the Photino Mass from Cosmology*, *Phys. Rev. Lett.* **50** (1983) 1419, [Erratum: *Phys. Rev. Lett.* 103 (2009) 099905].
- [10] J. R. Ellis, J. S. Hagelin, D. V. Nanopoulos, K. A. Olive, and M. Srednicki, *Supersymmetric Relics from the Big Bang*, *Nucl. Phys. B* **238** (1984) 453.
- [11] D. Albornoz Vásquez, G. Bélanger, and C. Böhm, *Revisiting light neutralino scenarios in the MSSM*, *Phys. Rev. D* **84** (2011) 095015, [arXiv:1108.1338 \[hep-ph\]](https://arxiv.org/abs/1108.1338).
- [12] G. Belanger, F. Boudjema, A. Cottrant, A. Pukhov, and A. Semenov, *WMAP constraints on SUGRA models with non-universal gaugino masses and prospects for direct detection*, *Nucl. Phys. B* **706** (2005) 411, [arXiv:hep-ph/0407218](https://arxiv.org/abs/hep-ph/0407218).
- [13] S. King, J. Roberts, and D. Roy, *Natural dark matter in SUSY GUTs with non-universal gaugino masses*, *JHEP* **10** (2007) 106, [arXiv:0705.4219 \[hep-ph\]](https://arxiv.org/abs/0705.4219).
- [14] M. Dine and W. Fischler, *A Phenomenological Model of Particle Physics Based on Supersymmetry*, *Phys. Lett. B* **110** (1982) 227.
- [15] L. Alvarez-Gaume, M. Claudson, and M. B. Wise, *Low-Energy Supersymmetry*, *Nucl. Phys. B* **207** (1982) 96.
- [16] C. R. Nappi and B. A. Ovrut, *Supersymmetric Extension of the $SU(3) \times SU(2) \times U(1)$ Model*, *Phys. Lett. B* **113** (1982) 175.
- [17] L. Randall and R. Sundrum, *Out of this world supersymmetry breaking*, *Nucl. Phys. B* **557** (1999) 79, [arXiv:hep-th/9810155](https://arxiv.org/abs/hep-th/9810155).
- [18] G. F. Giudice, M. A. Luty, H. Murayama, and R. Rattazzi, *Gaugino mass without singlets*, *JHEP* **12** (1998) 027, [arXiv:hep-ph/9810442](https://arxiv.org/abs/hep-ph/9810442).
- [19] ATLAS Collaboration, *Search for the electroweak production of supersymmetric particles in $\sqrt{s} = 8$ TeV pp collisions with the ATLAS detector*, *Phys. Rev. D* **93** (2016) 052002, [arXiv:1509.07152 \[hep-ex\]](https://arxiv.org/abs/1509.07152).
- [20] CMS Collaboration, *Searches for electroweak production of charginos, neutralinos, and sleptons decaying to leptons and W , Z , and Higgs bosons in pp collisions at 8 TeV*, *Eur. Phys. J. C* **74** (2014) 3036, [arXiv:1405.7570 \[hep-ex\]](https://arxiv.org/abs/1405.7570).
- [21] CMS Collaboration, *Search for supersymmetry in events with a τ lepton pair and missing transverse momentum in proton–proton collisions at $\sqrt{s} = 13$ TeV*, *JHEP* **11** (2018) 151, [arXiv:1807.02048 \[hep-ex\]](https://arxiv.org/abs/1807.02048).

[22] The LEP SUSY Working Group and the ALEPH, DELPHI, L3 and OPAL experiments notes LEPSUSYWG/01-03.1, 04-01.1, <http://lepsusy.web.cern.ch/lepsusy/Welcome.html>.

[23] ALEPH Collaboration, S. Schael, et al., *Absolute mass lower limit for the lightest neutralino of the MSSM from e^+e^- data at \sqrt{s} up to 209 GeV*, *Phys. Lett. B* **583** (2004) 247.

[24] DELPHI Collaboration, J. Abdallah, et al., *Searches for supersymmetric particles in e^+e^- collisions up to 208 GeV and interpretation of the results within the MSSM*, *Eur. Phys. J. C* **31** (2003) 421.

[25] L3 Collaboration, M. Acciarri, et al., *Search for charginos and neutralinos in e^+e^- collisions at $\sqrt{s} = 189$ GeV*, *Phys. Lett. B* **472** (2000) 420.

[26] OPAL Collaboration, G. Abbiendi, et al., *Search for chargino and neutralino production at $\sqrt{s} = 192$ GeV to 209 GeV at LEP*, *Eur. Phys. J. C* **35** (2004) 1.

[27] ATLAS Collaboration, *The ATLAS Experiment at the CERN Large Hadron Collider*, *JINST* **3** (2008) S08003.

[28] B. Abbott et al., *Production and integration of the ATLAS Insertable B-Layer*, *JINST* **13** (2018) T05008, [arXiv:1803.00844 \[physics.ins-det\]](https://arxiv.org/abs/1803.00844).

[29] ATLAS Collaboration, *Performance of the ATLAS Trigger System in 2015*, *Eur. Phys. J. C* **77** (2017) 317, [arXiv:1611.09661 \[hep-ex\]](https://arxiv.org/abs/1611.09661).

[30] ATLAS Collaboration, *Luminosity determination in pp collisions at $\sqrt{s} = 8$ TeV using the ATLAS detector at the LHC*, *Eur. Phys. J. C* **76** (2016) 653, [arXiv:1608.03953 \[hep-ex\]](https://arxiv.org/abs/1608.03953).

[31] G. Avoni et al., *The new LUCID-2 detector for luminosity measurement and monitoring in ATLAS*, *JINST* **13** (2018) 07017.

[32] ATLAS Collaboration, *The ATLAS Simulation Infrastructure*, *Eur. Phys. J. C* **70** (2010) 823, [arXiv:1005.4568 \[physics.ins-det\]](https://arxiv.org/abs/1005.4568).

[33] S. Agostinelli et al., *GEANT4: A simulation toolkit*, *Nucl. Instrum. Meth. A* **506** (2003) 250.

[34] T. Sjöstrand, S. Mrenna, and P. Z. Skands, *A brief introduction to PYTHIA 8.1*, *Comput. Phys. Commun.* **178** (2008) 852, [arXiv:0710.3820 \[hep-ph\]](https://arxiv.org/abs/0710.3820).

[35] ATLAS Collaboration, *The Pythia 8 A3 tune description of ATLAS minimum bias and inelastic measurements incorporating the Donnachie–Landshoff diffractive model*, ATL-PHYS-PUB-2016-017, 2016, <https://cds.cern.ch/record/2206965>.

[36] A. D. Martin, W. J. Stirling, R. S. Thorne and G. Watt, *Parton distributions for the LHC*, *Eur. Phys. J. C* **63** (2009) 189, [arXiv:0901.0002 \[hep-ph\]](https://arxiv.org/abs/0901.0002).

[37] T. Gleisberg et al., *Event generation with SHERPA 1.1*, *JHEP* **02** (2009) 007, [arXiv:0811.4622 \[hep-ph\]](https://arxiv.org/abs/0811.4622).

[38] S. Höche, F. Krauss, M. Schonherr, and F. Siegert, *QCD matrix elements + parton showers: The NLO case*, *JHEP* **04** (2013) 027, [arXiv:1207.5030 \[hep-ph\]](https://arxiv.org/abs/1207.5030).

[39] T. Gleisberg and S. Höche, *Comix, a new matrix element generator*, *JHEP* **12** (2008) 039, [arXiv:0808.3674 \[hep-ph\]](https://arxiv.org/abs/0808.3674).

[40] F. Caccioli, P. Maierhofer, and S. Pozzorini, *Scattering Amplitudes with Open Loops*, *Phys. Rev. Lett.* **108** (2012) 111601, [arXiv:1111.5206 \[hep-ph\]](https://arxiv.org/abs/1111.5206).

[41] A. Denner, S. Dittmaier, and L. Hofer, *Collier: a fortran-based Complex One-Loop Library in Extended Regularizations*, *Comput. Phys. Commun.* **212** (2017) 220–238, [arXiv:1604.06792](https://arxiv.org/abs/1604.06792) [hep-ph].

[42] S. Schumann and F. Krauss, *A Parton shower algorithm based on Catani-Seymour dipole factorisation*, *JHEP* **03** (2008) 038, [arXiv:0709.1027](https://arxiv.org/abs/0709.1027) [hep-ph].

[43] R. D. Ball et al., *Parton distributions for the LHC Run II*, *JHEP* **04** (2015) 040, [arXiv:1410.8849](https://arxiv.org/abs/1410.8849) [hep-ph].

[44] S. Catani, L. Cieri, G. Ferrera, D. de Florian, and M. Grazzini, *Vector boson production at hadron colliders: a fully exclusive QCD calculation at NNLO*, *Phys. Rev. Lett.* **103** (2009) 082001, [arXiv:0903.2120](https://arxiv.org/abs/0903.2120) [hep-ph].

[45] S. Höche, F. Krauss, M. Schonherr, and F. Siegert, *A critical appraisal of NLO+PS matching methods*, *JHEP* **09** (2012) 049, [arXiv:1111.1220](https://arxiv.org/abs/1111.1220) [hep-ph].

[46] S. Catani, F. Krauss, R. Kuhn, and B. R. Webber, *QCD matrix elements + parton showers*, *JHEP* **11** (2001) 063, [arXiv:hep-ph/0109231](https://arxiv.org/abs/hep-ph/0109231).

[47] S. Höche, F. Krauss, S. Schumann, and F. Siegert, *QCD matrix elements and truncated showers*, *JHEP* **05** (2009) 053, [arXiv:0903.1219](https://arxiv.org/abs/0903.1219) [hep-ph].

[48] S. Alioli, P. Nason, C. Oleari, and E. Re, *A general framework for implementing NLO calculations in shower Monte Carlo programs: the POWHEG BOX*, *JHEP* **06** (2010) 043, [arXiv:1002.2581](https://arxiv.org/abs/1002.2581) [hep-ph].

[49] ATLAS Collaboration, *ATLAS Pythia 8 tunes to 7 TeV data*, ATL-PHYS-PUB-2014-021, 2014, <https://cds.cern.ch/record/1966419>.

[50] J. Pumplin et al., *New generation of parton distributions with uncertainties from global QCD analysis*, *JHEP* **0207** (2002) 012, [arXiv:hep-ph/0201195](https://arxiv.org/abs/hep-ph/0201195) [hep-ph].

[51] M. Czakon and A. Mitov, *Top++: A program for the calculation of the top-pair cross-section at hadron colliders*, *Comput. Phys. Commun.* **185** (2014) 2930, [arXiv:1112.5675](https://arxiv.org/abs/1112.5675) [hep-ph].

[52] N. Kidonakis, *Two-loop soft anomalous dimensions for single top quark associated production with a W- or H-*, *Phys. Rev. D* **82** (2010) 054018, [arXiv:1005.4451](https://arxiv.org/abs/1005.4451) [hep-ph].

[53] P. Kant et al., *HatHor for single top-quark production: Updated predictions and uncertainty estimates for single top-quark production in hadronic collisions*, *Comput. Phys. Commun.* **191** (2015) 74, [arXiv:1406.4403](https://arxiv.org/abs/1406.4403) [hep-ph].

[54] J. Alwall et al., *The automated computation of tree-level and next-to-leading order differential cross sections, and their matching to parton shower simulations*, *JHEP* **07** (2014) 079, [arXiv:1405.0301](https://arxiv.org/abs/1405.0301) [hep-ph].

[55] R. D. Ball et al., *Parton distributions with LHC data*, *Nucl. Phys. B* **867** (2013) 244, [arXiv:1207.1303](https://arxiv.org/abs/1207.1303) [hep-ph].

[56] A. Lazopoulos, T. McElmurry, K. Melnikov, and F. Petriello, *Next-to-leading order QCD corrections to $t\bar{t}Z$ production at the LHC*, *Phys. Lett. B* **666** (2008) 62, [arXiv:0804.2220](https://arxiv.org/abs/0804.2220) [hep-ph].

[57] J. M. Campbell and R. K. Ellis, *$t\bar{t}W^{+-}$ production and decay at NLO*, *JHEP* **07** (2012) 052, [arXiv:1204.5678](https://arxiv.org/abs/1204.5678) [hep-ph].

[58] D. J. Lange, *The EvtGen particle decay simulation package*, *Nucl. Instrum. Meth. A* **462** (2001) 152.

[59] L. Lönnblad and S. Prestel, *Matching tree-level matrix elements with interleaved showers*, *JHEP* **03** (2012) 019, [arXiv:1109.4829 \[hep-ph\]](https://arxiv.org/abs/1109.4829).

[60] B. Fuks, M. Klasen, D. R. Lamprea, and M. Rothering, *Gaugino production in proton-proton collisions at a center-of-mass energy of 8 TeV*, *JHEP* **10** (2012) 081, [arXiv:1207.2159 \[hep-ph\]](https://arxiv.org/abs/1207.2159).

[61] B. Fuks, M. Klasen, D. R. Lamprea, and M. Rothering, *Precision predictions for electroweak superpartner production at hadron colliders with Resummino*, *Eur. Phys. J. C* **73** (2013) 2480, [arXiv:1304.0790 \[hep-ph\]](https://arxiv.org/abs/1304.0790).

[62] G. Bozzi, B. Fuks, and M. Klasen, *Threshold Resummation for Slepton-Pair Production at Hadron Colliders*, *Nucl. Phys. B* **777** (2007) 157, [arXiv:hep-ph/0701202 \[hep-ph\]](https://arxiv.org/abs/hep-ph/0701202).

[63] B. Fuks, M. Klasen, D. R. Lamprea, and M. Rothering, *Revisiting slepton pair production at the Large Hadron Collider*, *JHEP* **01** (2014) 168, [arXiv:1310.2621 \[hep-ph\]](https://arxiv.org/abs/1310.2621).

[64] J. Fiaschi and M. Klasen, *Slepton pair production at the LHC in NLO+NLL with resummation-improved parton densities*, *JHEP* **03** (2018) 094, [arXiv:1801.10357 \[hep-ph\]](https://arxiv.org/abs/1801.10357).

[65] ATLAS Collaboration, *Vertex Reconstruction Performance of the ATLAS Detector at $\sqrt{s} = 13$ TeV*, ATL-PHYS-PUB-2015-026, 2015, <https://cds.cern.ch/record/2037717>.

[66] ATLAS Collaboration, *Topological cell clustering in the ATLAS calorimeters and its performance in LHC Run 1*, *Eur. Phys. J. C* **77** (2017) 490, [arXiv:1603.02934 \[hep-ex\]](https://arxiv.org/abs/1603.02934).

[67] M. Cacciari, G. P. Salam, and G. Soyez, *The anti- k_T jet clustering algorithm*, *JHEP* **04** (2008) 063, [arXiv:0802.1189 \[hep-ph\]](https://arxiv.org/abs/0802.1189).

[68] M. Cacciari, G. P. Salam, and G. Soyez, *FastJet User Manual*, *Eur. Phys. J. C* **72** (2012) 1896, [arXiv:1111.6097 \[hep-ph\]](https://arxiv.org/abs/1111.6097).

[69] ATLAS Collaboration, *Jet energy scale measurements and their systematic uncertainties in proton-proton collisions at $\sqrt{s} = 13$ TeV with the ATLAS detector*, *Phys. Rev. D* **96** (2017) 072002, [arXiv:1703.09665 \[hep-ex\]](https://arxiv.org/abs/1703.09665).

[70] M. Cacciari and G. P. Salam, *Pileup subtraction using jet areas*, *Phys. Lett. B* **659** (2008) 119, [arXiv:0707.1378](https://arxiv.org/abs/0707.1378).

[71] ATLAS Collaboration, *Tagging and suppression of pileup jets with the ATLAS detector*, ATL-CONF-2014-018, 2014, <https://cds.cern.ch/record/1700870>.

[72] ATLAS Collaboration, *Measurements of b -jet tagging efficiency with the ATLAS detector using $t\bar{t}$ events at $\sqrt{s} = 13$ TeV*, *JHEP* **08** (2018) 089, [arXiv:1805.01845 \[hep-ex\]](https://arxiv.org/abs/1805.01845).

[73] ATLAS Collaboration, *Performance of b -jet identification in the ATLAS experiment*, *JINST* **11** (2016) P04008, [arXiv:1512.01094 \[hep-ex\]](https://arxiv.org/abs/1512.01094).

[74] ATLAS Collaboration, *Expected performance of the ATLAS b -tagging algorithms in Run-2*, ATL-PHYS-PUB-2015-022, 2015, <https://cds.cern.ch/record/2037697>.

[75] ATLAS Collaboration, *Optimisation of the ATLAS b -tagging performance for the 2016 LHC Run*, ATL-PHYS-PUB-2016-012, 2016, <https://cds.cern.ch/record/2160731>.

[76] ATLAS Collaboration, *Electron reconstruction and identification in the ATLAS experiment using the 2015 and 2016 LHC proton–proton collision data at $\sqrt{s} = 13$ TeV*, *Eur. Phys. J.* (2019), [arXiv:1902.04655 \[hep-ex\]](https://arxiv.org/abs/1902.04655).

[77] ATLAS Collaboration, *Muon reconstruction performance of the ATLAS detector in proton–proton collision data at $\sqrt{s} = 13$ TeV*, *Eur. Phys. J. C* **76** (2016) 292, [arXiv:1603.05598 \[hep-ex\]](https://arxiv.org/abs/1603.05598).

[78] ATLAS Collaboration, *Electron efficiency measurements with the ATLAS detector using the 2015 LHC proton–proton collision data*, ATLAS-CONF-2016-024, 2016, <https://cds.cern.ch/record/2157687>.

[79] ATLAS Collaboration, *Measurement of the tau lepton reconstruction and identification performance in the ATLAS experiment using pp collisions at $\sqrt{s} = 13$ TeV*, ATLAS-CONF-2017-029, 2017, <https://cds.cern.ch/record/2261772>.

[80] ATLAS Collaboration, *Identification and energy calibration of hadronically decaying tau leptons with the ATLAS experiment in pp collisions at $\sqrt{s} = 8$ TeV*, *Eur. Phys. J. C* **75** (2015) 303, [arXiv:1412.7086 \[hep-ex\]](https://arxiv.org/abs/1412.7086).

[81] ATLAS Collaboration, *Performance of missing transverse momentum reconstruction with the ATLAS detector using proton–proton collisions at $\sqrt{s} = 13$ TeV*, *Eur. Phys. J. C* **78** (2018) 903, [arXiv:1802.08168 \[hep-ex\]](https://arxiv.org/abs/1802.08168).

[82] ATLAS Collaboration, *The ATLAS Tau Trigger in Run 2*, ATLAS-CONF-2017-061, 2017, <https://cds.cern.ch/record/2274201>.

[83] C. G. Lester and D. J. Summers, *Measuring masses of semi-invisibly decaying particles pair produced at hadron colliders*, *Phys. Lett. B* **463** (1999) 99, [arXiv:hep-ph/9906349](https://arxiv.org/abs/hep-ph/9906349).

[84] A. Barr, C. Lester, and P. Stephens, *A variable for measuring masses at hadron colliders when missing energy is expected; m_{T2} : the truth behind the glamour*, *J. Phys. G* **29** (2003) 2343, [arXiv:hep-ph/0304226](https://arxiv.org/abs/hep-ph/0304226).

[85] G. Cowan, K. Cranmer, E. Gross, and O. Vitells, *Asymptotic formulae for likelihood-based tests of new physics*, *Eur. Phys. J. C* **71** (2011) 1554, [arXiv:1007.1727 \[physics.data-an\]](https://arxiv.org/abs/1007.1727), [Erratum: *Eur. Phys. J. C* **73** (2013) 2501].

[86] D. Tovey, *On measuring the masses of pair-produced semi-invisibly decaying particles at hadron colliders*, *JHEP* **04** (2008) 034, [arXiv:hep-ph/0802.2879](https://arxiv.org/abs/hep-ph/0802.2879).

[87] ATLAS Collaboration, *Measurement of the Inelastic Proton-Proton Cross Section at $\sqrt{s} = 13$ TeV with the ATLAS Detector at the LHC*, *Phys. Rev. Lett.* **117** (2016) 182002, [arXiv:1606.02625 \[hep-ex\]](https://arxiv.org/abs/1606.02625).

[88] J. Butterworth et al., *PDF4LHC recommendations for LHC Run II*, *J. Phys. G* **43** (2016) 023001, [arXiv:1510.03865 \[hep-ex\]](https://arxiv.org/abs/1510.03865).

[89] M. Baak et al., *HistFitter software framework for statistical data analysis*, *Eur. Phys. J. C* **75** (2015) 153, [arXiv:1410.1280 \[hep-ex\]](https://arxiv.org/abs/1410.1280).

[90] A. L. Read, *Presentation of search results: the CLs technique*, *J. Phys. G* **28** (2002) 2693.